J Comput Aided Mol Des (2012) 26:1111–1126
DOI 10.1007/s10822-012-9602-x

Mapping of the interaction sites of galanthamine: a quantitative analysis through pairwise potentials and quantum chemistry

Nicolas Galland · Soleymane Kone · Jean-Yves Le Questel

Received: 10 May 2012 / Accepted: 5 September 2012 / Published online: 13 September 2012

Abstract A quantitative analysis of the interaction sites of the anti-Alzheimer drug galanthamine with molecular probes (water and benzene molecules) representative of its surroundings in the binding site of acetylcholinesterase (AChE) has been realized through pairwise potentials calculations and quantum chemistry. This strategy allows a full and accurate exploration of the galanthamine potential energy surface of interaction. Significantly different results are obtained according to the distances of approaches between the various molecular fragments and the conformation of the galanthamine *N*-methyl substituent. The geometry of the most relevant complexes has then been fully optimized through MPWB1K/6-31 + G(d,p) calculations, final energies being recomputed at the LMP2/aug-cc-pVTZ(-f) level of theory. Unexpectedly, galanthamine is found to interact mainly from its hydrogen-bond donor groups. Among those, CH groups in the vicinity of the ammonium group are prominent. The trends obtained provide rationales to the predilection of the equatorial orientation of the galanthamine *N*-methyl substituent for binding to AChE. The analysis of the interaction energies pointed out the independence between the various interaction sites and the rigid character of galanthamine. The comparison between the cluster calculations and the crystallographic observations in galanthamine-AChE co-crystals allows the validation of the theoretical methodology. In particular, the positions of several water molecules appearing as strongly conserved in galanthamine-AChE co-crystals are predicted by the calculations. Moreover, the experimental position and orientation of lateral chains of functionally important aminoacid residues are in close agreement with the ones predicted theoretically. Our study provides relevant information for a rational drug design of galanthamine based AChE inhibitors.

Keywords Galanthamine · Hydrogen bonding · Quantum chemistry · Acetylcholinesterase

Introduction

The elderly population increase observed in the occidental world induces a concomitant increase of age-related pathologies among which Alzheimer-Disease (AD) is one of the most important afflictions. While the etiology of the disease is still unknown, the search of an effective therapeutic treatment of this senile syndrome is of great importance because of its social and health public consequences. AD is accompanied by a severe alteration of the cholinergic system. Historically, the relation between the observed cholinergic dysfunction and AD severity provided a rationale for the development of cholinergic therapeutics used in the treatment of AD. These treatments aim at targeting (1) the inhibition of acetylcholinesterase (AChE) in the brain, which results in an elevation of the acetylcholine (ACh) concentration and therefore in the

Electronic supplementary material The online version of this article (doi:10.1007/s10822-012-9602-x) contains supplementary material, which is available to authorized users.

N. Galland · J.-Y. Le Questel (✉)
UMR CNRS 6230, Chimie Et Interdisciplinarité: Synthèse, Analyse, Modélisation (CEISAM), UFR Sciences & Techniques, Université de Nantes, 2, rue de la Houssinière, BP 92208, 44322 NANTES Cedex 3, France
e-mail: Jean-Yves.Le-Questel@univ-nantes.fr

S. Kone
Laboratoire de Chimie Organique Structurale, UFR SSMT, Université d'Abidjan-Cocody, 22, BP 582, Abidjan 02, Ivory Coast

activation of the cholinergic transmission [1–3] (2) the activation of nicotinic receptors which is enhanced with allosterically potentiating ligands through nicotinic agonists [4, 5]. Despite the fact that the effectiveness of AChE inhibitors has been questioned, they are still the first and the most developed drugs approved for the symptomatic treatment of AD patients with mild to moderate dementia. AChE inhibitors can be natural substances, such as the alkaloids physostigmine [6, 7] and huperzine A [8, 9], others arise from organic synthesis, such as tacrine (Cognex®) or E2020 (Aricept®) [10, 11]. Furthermore, an NMDA (*N*-methyl-D-aspartate) receptor antagonist, Ebixa® (memantine) has been launched on the market [12]. Among these compounds, galanthamine deserves a special attention because of its dual mode of action, as an inhibitor of AChE and as an allosteric modulator of nAChRs. Moreover, it exhibits less toxicity than tacrine, rivastigmine and donepezil. Indeed, galanthamine remains a lead compound for the development of new inhibitors [13–15].

The importance of the knowledge of the 3D structure of AChE in rational drug design has led to a great number of structural studies recently reviewed [16, 17]. For the same reasons, theoretical investigations aimed at rationalizing the binding of classical as well as new potential inhibitors to AChE have been reported [18–20]. The structural studies have revealed that the active site of AChE is buried close to the bottom of a deep and narrow gorge, which is lined by 14 conserved aromatic residues, the rings of which make up 70 % of the gorge surface. Among those, W84 and F330 contribute to the so-called catalytic anionic site (CAS), Y70, Y121 and W279 to the peripheral anionic site (PAS). A recent X-ray and molecular dynamics study has pointed out the diversity, in terms of flexibility degree, of these various aromatic amino-acid side chains [21]. Another notable structural feature of AChE is its "conformational plasticity", which permits the entry of bulky and rigid inhibitors like galanthamine in the CAS [22, 23]. The observation of clusters of buried water molecules strongly conserved in various 3D structures (native and inhibitor complexes) of AChE has been suggested to play a possible role of lubricant, allowing large-amplitude fluctuations of the loop structures forming the gorge wall and explaining the remarkable plasticity of the enzyme [24]. Water molecules are also strongly conserved in the active site of AChE, but their comparison have been more difficult than for buried water molecules since different inhibitors displace different water molecules [24]. Nevertheless, these observations are consistent with an important structural and functional role of water in AChE. Steered molecular dynamic (SMD) simulations have confirmed the lubricant role of water molecules in the entering or leaving of the binding gorge of HuperzineA [25]. In this context, the molecular modeling investigations of McCammon's group have allowed a deep understanding of AChE reactivity and selectivity [26–32].

The dual biological activity of galanthamine and its position of lead compound for the development of new anti-Alzheimer drugs have led us to complete our previous investigations [33–35] by a comprehensive study aimed at mapping quantitatively the various interaction sites of this important alkaloid. In the present work, we investigate the galanthamine interactions through the analysis of its complexation with molecular fragments representative of its surroundings in AChE, namely water and benzene molecules. We have analysed in detail in a previous study the main structural features of galanthamine (Fig. 1) in its neutral (GAL) and protonated ($GALH^+$) forms and shown that the molecule must exist as a mixture of equatorial and axial *N*-methyl isomers [34, 35]. Furthermore, we have pointed out the flexibility of the hydroxyl and methoxy groups orientation according to the chemical environment. In particular, we have shown the predilection for a conformation stabilized by an intramolecular $O_{15}H_{16}\ldots O_4$ hydrogen bond (HB) in the gas phase, this orientation remaining the most observed in crystalline environments [33]. In AChE, however, the OH group is engaged in a HB interaction with (1) a water molecule having a well-defined position systematically observed in the galanthamine-AChE complexes (2) the carboxylate group of a glutamate residue (Glu199) [15, 22, 23]. Another noticeable feature of galanthamine in the AChE environment is the fact that an sp^3 oxygen atom is almost always observed in strong interaction with the $N_{11}H^+$ of the tetrahydroazepine ring. Based on these structural trends, we have considered for the present investigation the chemical form of $GALH^+$ which appears the most relevant, that is to say the complex between protonated galanthamine and a water molecule (called GALw hereafter). In this complex, the positive charge of the $N_{11}H^+$ is partially neutralized by the water molecule [33]. To take into account the main structural features of $GALH^+$ in GALw, a total of six conformers of the molecule have therefore been considered in the present work. They correspond to the axial and equatorial isomers of the *N*-methyl substituent and for each of them, to the three orientations of the OH group (one giving rise to the intramolecular $O_{15}H_{16}\ldots O_4$ HB, the others corresponding to the *trans* and *gauche* orientation of the hydroxyl with respect to the C_5–C_6 bond) [34]. The potential energy surfaces of interaction of each GALw structure have been fully explored using an intermolecular anisotropic atom–atom model potential based on an accurate distributed multipole analysis (DMA) model for the dominant electrostatic interaction. Full geometry optimizations have then been carried out using the MPWB1K density functional, final energies being recomputed at the local MP2 level of theory.

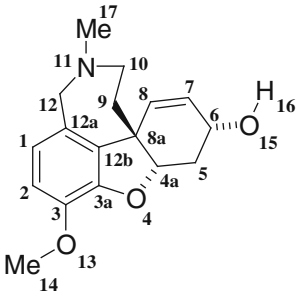

Fig. 1 Chemical structure and numbering of galanthamine

In this paper, after a presentation of the theoretical methods used for the cluster calculations, the results obtained for the complexation of GALw by one water or one benzene "probe" molecules are reported and discussed. Third body effects consecutive to the complexation by one further water or benzene molecule are then analyzed. The interaction sites of galanthamine, identified in terms of position and chemical nature, are evaluated using energetic (binding energies) and statistic criteria. Finally, the theoretical results are compared to crystallographic observations from galanthamine-AChE co-crystals. The good agreement obtained between our results and the interactions of galanthamine observed by X-ray crystallography in the AChE binding site illustrates the interest of this approach for the quantitative discrimination of the interaction sites of ligands of therapeutic interest.

Methods

The various steps of the computational methodology we have used, together with their corresponding levels of theory and the systems investigated are indicated on Fig. 2.

Model intermolecular potential calculations

The model intermolecular potential calculations were carried out assuming that there is no relaxation of the geometry of each monomer during the complexation. The monomer geometries were kept fixed at the MPWB1K/6-31 + G(d,p) optimized geometries. To obtain the binding energy ΔE, the minimum in the potential energy U of the complex is adjusted by the zero-point vibrational energy (ZPVE) contribution calculated from the harmonic intermolecular vibrational frequencies. The model potential, dubbed MP2fit/DMA [36], consists of repulsion and dispersion terms augmented with a DMA model [37, 38] to describe the electrostatic interaction:

$$U_{MN} = \sum_{a\in M}\sum_{b\in N} A_{\alpha\beta}\,\exp(-B_{\alpha\beta}R_{\alpha\beta}) - \frac{C_{\alpha\beta}}{R_{ab}^6} + U^{DMA}(R_{ab},\Omega_{ab})$$

with

$$A_{\alpha\beta} = (A_{\alpha\alpha}A_{\beta\beta})^{1/2},\ B_{\alpha\beta} = \frac{1}{2}(B_{\alpha\alpha} + B_{\beta\beta}),\ C_{\alpha\beta} = (C_{\alpha\alpha}C_{\beta\beta})^{1/2} \quad (1)$$

The sum runs over the atoms a and b (of type α and β) of monomers M and N, respectively. The repulsion and dispersion parameters were empirically fitted to organic crystal structures, heats of sublimation and accurate ab initio data [36, 39–41]. The DMA electrostatic model includes all terms in the atom–atom multipole expansion up to R_{ab}^{-5}. It uses atomic multipoles up to hexadecapole derived from ab initio wavefunctions (MP2/6-311G(d,p) for the GALw conformers and the benzene molecule; MP2/6-311++G(2d,2p) for water molecule). The GDMA program [42] was used to compute the DMA models from the wavefunctions, and the model potential calculations on the complexes were carried out with the ORIENT program [43]. Comparable approaches have not only been tried and tested but have also been used recently for the theoretical study of intermolecular interactions of organic ligands such as phloroglucinol [44] and carbohydrates [45] and the binding of host–guest complexes [46].

The advantage of using the model potential is that we were able to scan thoroughly the potential energy surface (PES) of the systems studied by performing geometry optimizations from a large number of starting points. For each system (GALw + H_2O, GALw + $2H_2O$, GALw + C_6H_6, GALw + C_6H_6 + H_2O), 2,400 structures were generated with initial random orientations of the monomers. More precisely, we have defined for each of the six GALw conformers four categories of starting points based on the intermolecular distance: 100 structures were generated with a distance randomly initialized up to 15 Å (corresponding to a very long-range approach of the monomers), 100 structures with a distance randomly initialized up to 10 Å (long-range approach of the monomers), 100 structures with a distance randomly initialized up to 5 Å (medium-range approach) and finally 100 structures with a random distance smaller than 1 Å (short-range approach). From a statistical point of view, significant variations on the PES searching results were observed depending on the initial intermolecular distance (long-range vs. medium or short-range approaches). The agreement between the model potential and DFT/ab initio results showed that the model potential is enough robust to scan thoroughly the PES of the systems studied.

Electronic structure calculations

Owing to their excellent performance-to-cost ratio, the DFT methods constitute a very appealing approach, and among them the B3LYP functional is probably the most popular one. The MPWB1K functional, developed recently by Truhlar and Zhao [47], gives improved results compared

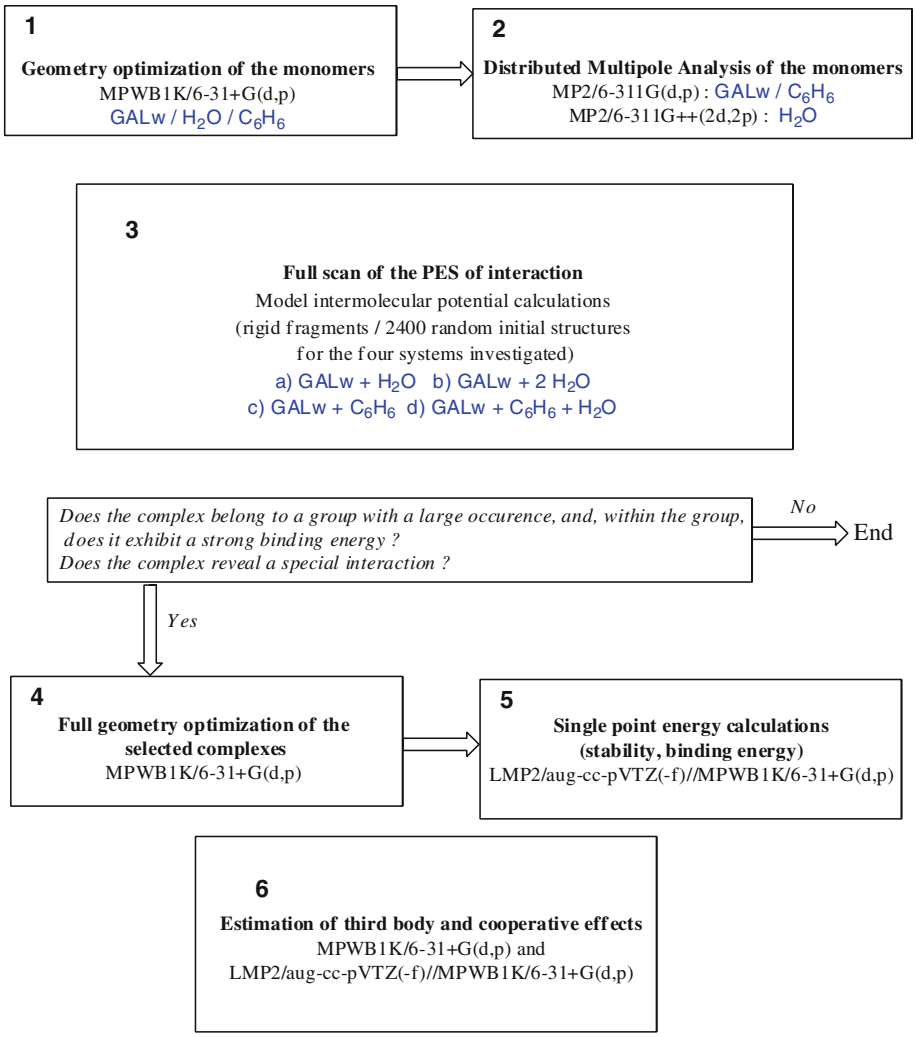

Fig. 2 Global organization of the computational methodology

with B3LYP for non-bonded interactions such as hydrogen bonding, hydrogen bonding to π acceptors and π–π stacking [47–51]. Starting from the interaction geometries optimized with the MP2fit/DMA potential, more accurate structures were obtained through full geometry optimizations carried out at the MPWB1K/6-31 + G(d,p) level of theory (see Optimized structures in Supporting Information). Note that the model intermolecular potential calculations used to explore the PES of interaction between the various monomers has led to several hundreds of structures (corresponding to a total of 9,600 starting points given the number of systems considered and the number of GALw conformers). Full geometry optimizations were restricted to a minority of them as (1) an optimization of all of them is not workable using DFT calculations, (2) it is evident that only a few of them have a true importance and (3) many structures share common energetic and structural features that characterize the interaction between the monomers. Most of the structures can then be brought together into a limited number of groups of complexes, categorized using the nature of the intermolecular interaction. We have applied three criteria to select the most representative ones:

- the complex must belong to a group with large occurrence,
- and within the group, the complex must exhibit a strong binding energy,
- and/or the complex reveals a special intermolecular interaction (such as multicentered HB or π–π stacking).

Using this procedure, more than 70 relevant complexes have been considered and their geometry fully optimized at the MPWB1K/6-31 + G(d,p) level of theory using the Gaussian03 suite of programs [52]. The harmonic vibrational frequencies were computed for the optimized geometries at the same level of theory to yield estimates of the ZPVE corrections to the total energy. The supermolecule approach was used to calculate binding energies,

which were furthermore corrected from basis set superposition error (BSSE) using the counterpoise methodology with monomer relaxation [53, 54]. Total and binding energies were recalculated using the local MP2 (LPM2) method [55, 56], which has been shown to yield an accuracy for relative energies that is superior to conventional MP2, due to elimination of BSSE [57–60]. Single point computations on MPWB1K/6-31 + G(d,p) geometries were performed at the LMP2/aug-cc-pVTZ(-f) level of theory (not corrected from BSSE) using the Jaguar7.0 program [61]. For the sake of simplicity, MPWB1K/6-31 + G(d,p) and LMP2/aug-cc-pVTZ(-f)//MPWB1K/6-31 + G(d,p) notations will be respectively replaced by MPWB1K and LMP2//MPWB1K throughout the text.

Estimation of third body and cooperative effects

The study of GALw + 2 H_2O and GALw + C_6H_6 + H_2O systems allows (1) examining the effect of a third molecule (water or benzene) on the GALw + H_2O and GALw + C_6H_6 systems, and (2) evaluating the influence of cooperative effects on the strength of the multiple interaction sites of galanthamine. Considering that the complexes are formed from *A* (GALw), *B* (water) and *C* (water or benzene) monomers, the binding energy is given by:

$$\begin{aligned}\Delta E = {} & \Delta E_{\mathrm{rel}}(A) + \Delta E_{\mathrm{rel}}(B) + \Delta E_{\mathrm{rel}}(C) + \Delta E_{2\mathrm{c}}(AB) \\ & + \Delta E_{2\mathrm{c}}(BC) + \Delta E_{2\mathrm{c}}(AC) + \Delta E_{3\mathrm{c}}(ABC)\end{aligned} \quad (2)$$

where ΔE_{rel} are the relaxation energies of monomers (*energy penalty* for distorting them from their isolated geometries to the ones in the complex), $\Delta E_{2\mathrm{c}}$ and $\Delta E_{3\mathrm{c}}$ are respectively the two- and three-body terms, defined as:

$$\begin{aligned}\Delta E_{2\mathrm{c}}(AB) &= E_{ABC}^{\alpha\cup\beta}(AB) - E_{ABC}^{\alpha}(A) - E_{ABC}^{\beta}(B) \\ \Delta E_{3\mathrm{c}}(ABC) &= E_{ABC}^{\alpha\cup\beta\cup\gamma}(ABC) \\ &\quad - \left[E_{ABC}^{\alpha}(A) + E_{ABC}^{\beta}(B) + E_{ABC}^{\gamma}(C)\right] \\ &\quad - \left[E_{ABC}^{\alpha\cup\beta}(AB) + E_{ABC}^{\beta\cup\gamma}(BC) + E_{ABC}^{\alpha\cup\gamma}(AC)\right]\end{aligned} \quad (3)$$

The molecular system considered is indicated in parentheses. The subscripts denote the geometry at which the energy is evaluated, while the superscripts denote if the energy is computed in the monomer, dimer or trimer basis set. For example, $E_{ABC}^{\alpha\cup\beta}(AB)$ is the energy of the dimer *AB*, at the geometry it has in the complex *ABC*, computed using the basis sets of *A* and *B* monomers ($\alpha\cup\beta$). In the case of MPWB1K calculations, the *n*-body terms must be corrected from BSSE. Following the scheme proposed by Xantheas [62], the two- and three-body terms are substituted with the BSSE corrected ones:

$$\begin{aligned}\Delta E_{2\mathrm{c}}(AB) &= E_{ABC}^{\alpha\cup\beta\cup\gamma}(AB) - E_{ABC}^{\alpha\cup\beta\cup\gamma}(A) - E_{ABC}^{\alpha\cup\beta\cup\gamma}(B) \\ \Delta E_{3\mathrm{c}}(ABC) &= E_{ABC}^{\alpha\cup\beta\cup\gamma}(ABC) \\ &\quad - \left[E_{ABC}^{\alpha\cup\beta\cup\gamma}(A) + E_{ABC}^{\alpha\cup\beta\cup\gamma}(B) + E_{ABC}^{\alpha\cup\beta\cup\gamma}(C)\right] \\ &\quad - \left[E_{ABC}^{\alpha\cup\beta\cup\gamma}(AB) + E_{ABC}^{\alpha\cup\beta\cup\gamma}(BC) + E_{ABC}^{\alpha\cup\beta\cup\gamma}(AC)\right]\end{aligned} \quad (4)$$

The *additive* part of the binding energy is usually defined as the sum of the two-body terms while higher order *n*-body terms constitute the *non-additive* part.

PDB

The environment of galanthamine in AChE has been investigated with the PyMol program [63] by selecting any residue within a sphere of 4 Å of any atom of galanthamine in the 1QTI PDB entry [64]. The comparison of the theoretical structures provided by the clusters calculations to the AChE binding site environment have been carried out with Pymol by overlaying the galanthamine structures. We shall limit this comparison by considering only the most representative results of the galanthamine environment in AChE, that is to say the complexes between GAlw and two water molecules, on the one hand, and the complexes between GAlw and one water and one benzene molecules, on the other hand. Furthermore, we will only consider in this discussion the conformational isomer of galanthamine that has been observed experimentally in the AChE binding site, that is to say characterized by an equatorial position of the methyl group carried by the ammonium N_{11} nitrogen, for which the methoxy group adopts a *trans* orientation with respect to the furanic oxygen O_4 and the hydroxyl group $O_{15}H_{16}$ adopts a *gauche* orientation with respect to the C_5C_6 bond [22, 64]. Among the *gauche* and *trans* conformations of the hydroxyl group, only the *gauche* one appears to allow HB interactions both with highly conserved water molecules and the carboxylate group of Glu199 [22, 64]. Finally, it is worth noticing that the galanthamine species considered in the present work (protonated galanthamine neutralized by a water molecule in interaction with the $N_{11}H^+$ ammonium group : GALw) is the one almost always observed in the AChE binding site [15, 22, 23, 64]. In fact, the only exception corresponds to a recent co-crystal of *N*-Piperidinopropyl-galanthamine with AChE, in which the amino nitrogen atom of the piperidine fragment, presumably protonated in this derivative owing to the difference of pK_a between the two nitrogen functions, appears in close contact with the N_{11} nitrogen atom of the tetrahydroazepine ring [15].

Results and discussion

Complexation of GALw by one water molecule

As stated previously, the numerous structures yielded by the model potential calculations can be brought together into a limited number of groups of complexes, categorized using the nature of the interaction between GALw and the water molecule (see Table S1 in Supporting Information). The geometrical characteristics of the complexes are displayed on Fig. 3. In the cases where the galanthamine *N*-methyl group is in axial position, one can observe that the initial distance between GALw and the water molecule has a strong influence on the diversity of structures yielded by the MP2fit/DMA calculations. For a long-range approach (Fig. 3a), two kinds of complexes are mostly present. The interaction between the free water molecule and the water molecule belonging to GALw (partial neutralization of $N_{11}H^+$) is responsible for the formation of almost 90 % of the complexes (see Movie 1 in Supporting Information). The H atoms of the aromatic ring C_2 and of the methoxy group C_{14} atoms interact with the water molecule in 6 % of the remaining complexes. For a short-range approach, the interaction sites of GALw are more systematically probed and a greater diversity of complexes is observed (Fig. 3b). In the case of a medium-range approach, an intermediate regime between the two preceding extremes is found. Overall, the main interaction site of GALw is the water molecule linked to the ammonium $N_{11}H^+$ group which acts as a hydrogen bond donor. This site is responsible for the formation of the higher proportion of complexes, whatever the value of the initial intermolecular distance. Regarding the structures where galanthamine exhibits no intramolecular HB (as in the AChE active site [33], Fig. 3c), the OH group obviously plays a major role as hydrogen bond donor (HBD) or acceptor (HBA). On average, it is involved in 30 % of the complexes formed via a short range approach.

When the galanthamine *N*-methyl group is in equatorial position (Fig. 3d–f), the diversity and the proportions of the various kinds of complexes yielded by the model potential calculations also strongly depend on the initial intermolecular distance. For a long-range approach, the main interaction site is composed by the H atoms carried by C atoms (C_{12} and C_{17}) directly linked to the positive nitrogen (responsible for the formation of up to 70 % of the complexes), while for a small initial intermolecular distance, the complexes driven by an interaction between the free water molecule and the water molecule belonging to GALw dominate (with a proportion about 30 %). Hence, we can't define an overall main interaction site. The important role of the OH group as HBD and HBA must specially be noticed in the cases where galanthamine exhibits no intramolecular $O_{15}H_{16}\ldots O_4$ HB. Indeed, numerous complexes are issued from the interaction of the water molecule with the hydroxyl.

Table 1 shows the binding energies calculated for the most significant complexes. The MPWB1K and LMP2 results are in overall good agreement, the MPWB1K binding energies being systematically more negative (on average by 3.1 kJ mol^{-1}). MP2fit/DMA calculations predict values either closer to LMP2 or to MPWB1K ones. For a same kind of interaction between GALw and the water molecule, we observe that the binding energy is well conserved whatever the position (axial or equatorial) of the galanthamine *N*-methyl substituent. The main sites of interaction are, by decreasing strength:

- the water molecule involved in the neutralization of the protonated nitrogen atom which acts as a HBD (binding energies ranging from −41 to −35 kJ mol^{-1}),
- the H atoms carried by C atoms (C_{10}, C_{12} and C_{17}) directly linked to the positive nitrogen which act as HBD (binding energies ranging from −29 to −24 kJ mol^{-1}),
- the hydroxyl group as HBD (average binding energies of −23 kJ mol^{-1}) or as HBA (average binding energies of −17 kJ mol^{-1}).

Furthermore, the O_4 and O_{13} atoms constitute another important HBA centre and their spatial proximity with $O_{15}H$ can give rise to multicentered HB interactions (see Movie 2 in Supporting Information). However, the resulting complexes do not show enhanced binding energies with respect to the complexes issued only of interactions with the OH group.

The relative energies of the selected complexes are also reported in Table 1. MPWB1K and LMP2 results are in good agreement for complexes with intramolecular $O_{15}H_{16}\ldots O_4$ HB, the average deviation being of 2.3 kJ mol^{-1}. For the remaining complexes (without $O_{15}H_{16}\ldots O_4$ HB), the stabilities are 6.2 kJ mol^{-1} stronger, on average, at the LMP2 level than at the MPWB1K one. This increasing discrepancy is most probably due to intramolecular BSSE, which is recognized to have a significant influence on the relative energies of conformations with different degrees of compactness [65–67]. While the *local* approximation in LMP2 eliminates BSSE to a large extent,[1] the intramolecular BSSE present in MPWB1K calculations leads to overestimate the stability of structures with intramolecular HB. Hence, the LMP2 relative

[1] Local correlation methods eliminate the incremental BSSE arising from electron correlation. Provided that the BSSE is small at the HF level of theory (i.e. a large basis set is used), the total BSSE is rendered practically negligible by the local correlation treatment [60, 61, 69]. On the example of the ax3:$O_{15}H$–O_4–O_{13} complex, the BSSE related to the binding energy is 1.2 and 0.2 kJ mol^{-1} at HF/aug-cc-pVTZ(-f)//MPWB1K/6-31 + G(d,p) and LMP2/aug-cc-pVTZ(-f)//MPWB1K/6-31 + G(d,p) levels of theory, respectively.

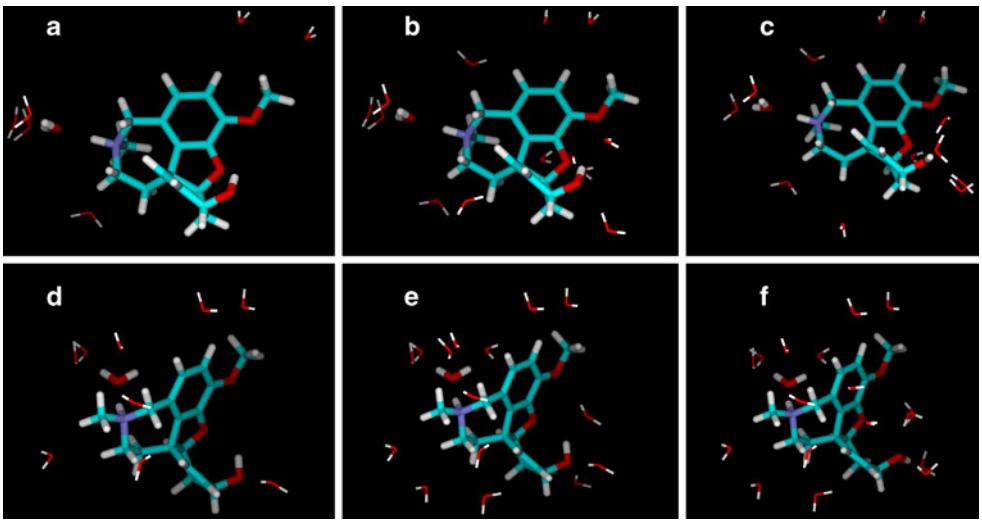

Fig. 3 Structures yielded by the MP2fit/DMA calculations for GALw + H_2O system. Each picture corresponds to 100 superimposed structures, GALw is represented using sticks and free water molecules using wireframe. **a**, **d** Correspond to a long-range approach of the water molecule and GALw while **b**, **c**, **e** and **f** correspond to a short-range approach. The galanthamine *N*-methyl group is in axial position in **a**–**c**, and in equatorial position in **d**–**f**. Three orientations of the galanthamine OH group are considered, one giving rise to the intramolecular $O_{15}H_{16}\ldots O_4$ HB (**a**, **b**, **d**, **e**), the others corresponding to the *trans* and *gauche* orientation of the hydroxyl with respect to the C_5–C_6 bond (**c**, **f**, respectively)

Table 1 Relative stabilities (δE kJ mol^{-1}) and binding energies (ΔE kJ mol^{-1}) of the most significant GALw + H_2O complexes calculated at various levels of theory

Complex[a]	δE		ΔE			Proportion[b]
	LMP2	MPWB1K	LMP2	MPWB1K	MP2fit/DMA	
eq1:H_2O	0	0	−34.5	−40.7	−37.1	30
ax1:H_2O	0.9	1.0	−35.8	−41.3	−39.7	95
eq1:$C_{10}H$–$C_{12}H$–$C_{17}H$	8.9	10.6	−25.6	−29.6	−24.7	15
eq1:$C_{12}H$–$C_{17}H$	8.9	11.9	−25.6	−28.3	−21.1	79
eq1:$C_{10}H$–$C_{17}H$	10.2	12.3	−24.3	−28.0	−22.4	12
eq3:$O_{15}H$	19.4	25.3	−22.2	−24.8	−28.9	22
eq1:C_2H	19.6	23.3	−14.9	−17.0	−13.4	16
eq2:$O_{15}H$	21.5	26.8	−20.6	−24.6	−29.1	17
ax3:$O_{15}H$–O_4–O_{13}	22.0	25.2	−23.7	−28.6	–[c]	20
eq3:O_{15}	22.7	31.9	−19.0	−18.3	−18.7	11
ax1:C_2H	23.5	26.9	−13.2	−14.8	−12.6	18
ax2:$O_{15}H$	24.4	30.5	−22.1	−25.0	−29.0	16
eq2:O_{15}	26.4	34.9	−15.7	−16.4	−19.6	15
ax2:O_{15}–O_4–O_{13}	31.2	39.1	−15.3	−16.5	−19.1	18
ax3:O_{15}	33.0	36.3	−12.8	−17.1	−14.8	13

[a] In the xn:i notation: x denotes the position (ax/eq) of the *N*-methyl substituent in the GAL subfragment; n denotes the conformation of the GAL subfragment with: intramolecular $O_{15}H_{16}\ldots O_4$ HB (1), a *trans* orientation of the $O_{15}H$ group with respect to the C_5–C_6 bond (2), a *gauche* orientation of the $O_{15}H$ group with respect to the C_5–C_6 bond (3); i denotes the GALw sites involved in the interaction with the water molecule

[b] From the four intermolecular approaches (see "Method", model intermolecular potential calculations), highest proportion yielded by the MP2fit/DMA calculations for the considered complex

[c] The geometry optimized using the MPWB1K functional differs notably from the structure yielded by the MP2fit/DMA calculations, hence their binding energies could not be compared

energies may be more reliable for the complexes without $O_{15}H_{16}...O_4$ HB. The latter appear mainly at high energies as the interactions with the free water molecule may not compensate for the energy rising due to the intramolecular HB cancellation. Finally, we find that the complexes yielded statistically in high proportions by the MP2fit/DMA calculations are not necessarily those that are the most stables or those that give rise to the strongest interactions.

Complexation of GALw by one benzene molecule

The geometrical characteristics of the complexes yielded by the MP2fit/DMA calculations are displayed on Fig. 4. As observed for the complexation with one water molecule, the diversity and the proportions of the different kinds of complexes yielded by the model potential calculations strongly depend on the initial distance between GALw and the benzene molecule (see Table S2 in Supporting Information). When the galanthamine *N*-methyl group is in axial position and for a long-range approach, the main interaction site of GALw is the water molecule linked to the ammonium $N_{11}H^+$ group (responsible for the formation of about 77 % of the complexes). Then, the complexes driven by an interaction with the H atom of the aromatic ring C_2 atom represent about 12 % of the whole. Another important amount of complexes is observed for galanthamine without intramolecular HB, the hydroxyl group being involved as an HBD in about 11 % of the complexes. In the case of a small initial intermolecular distance (Fig. 4a, b), more kinds of complexes are present in more equal proportions. In particular, complexes involving π–π stacking between the galanthamine aromatic ring and the benzene molecule appear in proportions ranging from 13 to 29 % depending on the orientation of the OH group. If the galanthamine *N*-methyl group is in equatorial position, we can define a main interaction site composed by the H atoms carried by C atoms (C_{10}, C_{12} and C_{17}) directly linked to the positive nitrogen. This interaction site is responsible for the formation of the largest amount of complexes, which can represent on average and for long-range approaches up to 79 % of the complexes. For a short-range approach between GALw and the benzene molecule (Fig. 4c, d), the interaction sites composed by the water molecule belonging to GALw and the galanthamine aromatic ring are also essential since they represent on average 39 % of the complexes.

Table 2 shows the binding energies calculated for the most significant complexes. Overall, the MPWB1K and LMP2 results are in good agreement if we do not consider the π–π staked complexes, the LMP2 binding energies being systematically more negative (on average by 3.0 kJ mol^{-1}).

For π–π stacked complexes, MPWB1K binding energies are on average 14.0 kJ mol^{-1} weaker than LMP2 ones. This may result from the fact that many conventional

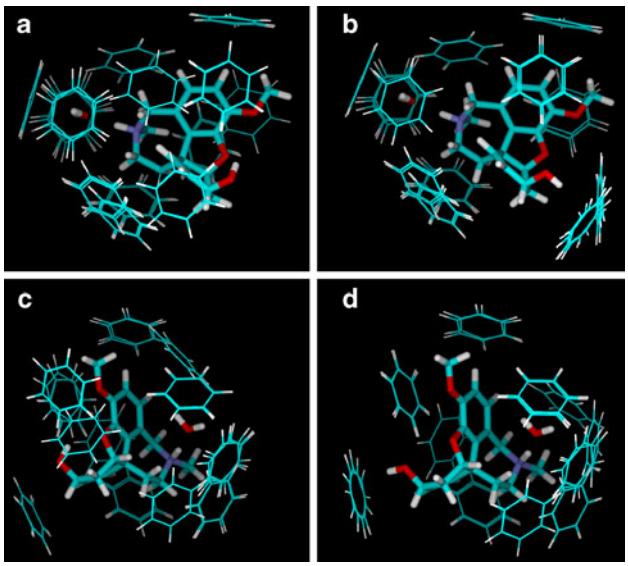

Fig. 4 Structures yielded by the MP2fit/DMA calculations for short-range approaches between GALw and a benzene molecule. Each picture corresponds to 100 superimposed structures, GALw is represented using sticks and benzene molecules using wireframe. The galanthamine *N*-methyl group is in axial position in **a** and **b**, and in equatorial position in **c** and **d**. Three orientations of the galanthamine OH group are considered, one giving rise to the intramolecular $O_{15}H_{16}...O_4$ HB (**a**, **c**), the others corresponding to the *trans* and *gauche* orientation of the hydroxyl with respect to the C_5–C_6 bond (**b**, **d**, respectively)

global hybrid DFT methods, including MPWB1K, are known to underestimate stacking interactions since they generally fail to describe accurately the (non-local) dispersion energy [49, 51, 69, 70]. On the other hand, the MP2fit/DMA calculations predict systematically the strongest binding energies, by 4.2 kJ mol^{-1} on average greater than the LMP2 ones.

The comparison between GALw + H_2O and GALw + C_6H_6 systems shows that for a same interaction site of GALw, the binding energies with the benzene molecule are weaker than with the water molecule. The main sites of interaction are by decreasing strength:

- the water molecule linked to the $N_{11}H^+$ group which acts as a HBD (average binding energies of −26 kJ mol^{-1}),
- the H atoms carried by C atoms linked to the positive nitrogen which act as HBD (binding energies ranging from −26 to −17 kJ mol^{-1}),
- the aromatic ring (binding energies over −20 kJ mol^{-1} at LMP2 level of theory).

The hydroxyl group and the H atom of the aromatic ring C_2 atom represent the weakest HBD sites: the respective average binding energies are −17 and −14 kJ mol^{-1}. The relative energies of the selected complexes are reported in Table 2. As the MPWB1K method underestimates the

Table 2 Relative stabilities (δE kJ mol^{-1}) and binding energies (ΔE kJ mol^{-1}) of the most significant GALw + C_6H_6 complexes calculated at various levels of theory

Complex[a]	δE		ΔE			Proportion[b]
	LMP2	MPWB1K	LMP2	MPWB1K	MP2fit/DMA	
eq1:H_2O	0.0	0.0	−30.3	−24.8	−33.7	24
eq1:$C_{10}H$–$C_{12}H$–$C_{17}H$	4.1	1.5	−26.2	−22.3	−29.1	83
ax1:C_9H–$C_{10}H$	7.5	6.6	−25.0	−18.8	−26.0	25
ax1:H_2O	10.5	−1.1	−22.0	−26.0	−25.3	86
eq3:arom. ring	11.0	20.5	−26.4	−13.3	−28.4	13
ax1:C_9H–$C_{10}H$–$C_{17}H$	12.4	7.6	−20.0	−16.5	−24.7	12
eq1:C_2H	15.0	12.0	−15.3	−12.0	−18.2	17
eq2:arom. ring	15.5	27.0	−22.4	−7.7	−28.1	16
ax1:C_2H	17.1	13.3	−15.3	−11.6	−17.7	18
eq3:$O_{15}H$	18.4	17.5	−19.0	−15.7	−23.6	29
eq2:$O_{15}H$	20.7	19.5	−17.2	−14.8	−22.8	28
ax3:arom. ring	20.7	28.3	−20.8	−8.4	−27.6	24
ax2:arom. ring	21.6	33.9	−20.6	−4.9	−27.3	29
ax3:$O_{15}H$	23.8	22.5	−17.7	−15.1	−23.5	30
ax2:$O_{15}H$	24.1	23.5	−18.1	−15.4	−22.7	24

[a] In the xn:i notation: x denotes the position (ax/eq) of the *N*-methyl substituent in the GAL subfragment; n denotes the conformation of the GAL subfragment with : intramolecular $O_{15}H_{16}$…O_4 HB (1), a *trans* orientation of the $O_{15}H$ group with respect to the C_5–C_6 bond (2), a *gauche* orientation of the $O_{15}H$ group with respect to the C_5–C_6 bond (3); i denotes the GALw site involved in the interaction with the water molecule

[b] From the four intermolecular approaches (see "Method", model intermolecular potential calculations), highest proportion yielded by the MP2fit/DMA calculations for the considered complex

energies of stacking interactions, the stabilities of π–π stacked complexes are underestimated at this level of theory. It is worth noticing that the complexes yielded statistically in high proportions by the MP2fit/DMA calculations are not necessarily those that are the most stable or those that give rise to the strongest interactions, like in the case of the GALw + H_2O system.

Effects of a third body

We have investigated the effect of introducing a third molecule (water or benzene), bound to GALw, on the behavior of the GALw + H_2O and GALw + C_6H_6 systems. The model potential calculations on both GALw + 2 H_2O and GALw + C_6H_6 + H_2O systems led to a large diversity of complexes, each kind of them being observed in small proportion. Hence, MP2fit/DMA results were analyzed on the basis of the nature of the various intermolecular interactions and their recurrence in order to uncover some trends (see Table S3 and Table S4 in Supporting Information). This analysis confirmed the trends observed for the complexation of GALw by one water or one benzene molecule, notably the key role played by the galanthamine *N*-methyl group. When the methyl substituent is axial, 83–96 % of the complexes exhibit intermolecular interactions with the water molecule belonging to GALw. In contrast, the interactions with this water molecule are involved in about 30 % of the complexes if the galanthamine *N*-methyl group is in equatorial position. The main interaction site is composed by the H atoms carried by C atoms (C_{10}, C_{12} and C_{17}) linked to the positive nitrogen. Indeed, it is involved in the formation of, at least, three quarters of the complexes. The other interaction sites are less sensitive to the *N*-methyl group conformation. It is worth noticing that (1) the H atoms of the aromatic ring C_2 and of the methoxy group C_{14} atoms give rise to intermolecular interactions in about 30 % of the complexes (2) for galanthamine without intramolecular HB, the hydroxyl group is involved in the same proportion of the complexes (∼30 % either as an HBA or an HBD). If one looks precisely at the GALw + C_6H_6 + H_2O system, he can observe that the competition between the free water and benzene molecules brings to light new aspects on GAL behavior. The comparison with the results obtained for the complexation of GALw by one benzene molecule shows that the benzene molecule is less regularly in interaction with the GALw main sites (the water molecule belonging to GALw if the galanthamine *N*-methyl group is in axial position, the H atoms carried by C_{10}, C_{12} and C_{17} atoms if the galanthamine *N*-methyl group is in equatorial position).

In return, the benzene molecule interacts more with peripheral sites like the HBD $O_{15}H$ group and the H atoms of the aromatic ring C_2 and of the methoxy group C_{14} atoms. In contrast, the behavior of the free water molecule appears almost not affected with respect to the results obtained for the complexation of GALw by one water molecule (only a slight increase of the proportion of complexes formed via an interaction with the H atoms of the C_2 and C_{14} atoms can be noticed).

The relative energies and binding energies calculated for the most significant complexes of the GALw + 2 H_2O and GALw + C_6H_6 + H_2O systems are reported, respectively, in Tables 3 and 4. The binding energies are ranging from −70 to −40 kJ mol^{-1} for the selected complexes. When GALw is complexed by two water molecules, the MPWB1K binding energies are systematically more negative than the LMP2 ones, as previously observed for the GALw + H_2O system. This is not the case when GALw is complexed by one water and one benzene molecule, the MPWB1K and LMP2 results being in close agreement. As expected, the complexes which exhibit the greater binding energies result from the combination of intermolecular interactions with the most favorable GALw sites described previously: the water molecule involved in the neutralization of the protonated nitrogen atom, the H atoms carried by C atoms linked to the positive nitrogen and the hydroxyl group. The water molecule belonging to GALw is systematically involved as HBD in the strongest and the most stable complexes. However, the complexes found in high proportions are neither those that are the most stables nor the ones that give rise to the strongest interactions. They correspond to structures that combine the most recurrent intermolecular interactions predicted by MP2fit/DMA calculations for the GALw + H_2O and GALw + C_6H_6 systems. Therefore, both from an energetic and a statistical point of view, our results show an increase of the trends observed from the study of the complexation of GALw by one water or one benzene molecule.

The magnitude of the *n*-body energy terms and their contribution to the binding energy of the selected complexes have been computed at LMP2 and MPWB1K levels of theory (see Table S5 and Table S6 in Supporting Information). The LMP2 and MPWB1K values of relaxation energies (ΔE_{rel}) and three-body terms (ΔE_{3c}) are in good agreement. Regarding the individual two-body terms (ΔE_{2c}) which correspond to intermolecular interactions between GALw and a water molecule, the MPWB1K values are systematically more negative than the LMP2 ones. The opposite is observed for the individual ΔE_{2c}(AC) terms which correspond to interactions between GALw and the benzene molecule. Clearly, the stability of the complexes is essentially due to additive effects. The total two-body term contributes on average to 95 % of the binding energy. For the majority of the selected complexes, the contribution of ΔE_{rel} is negligible. It is the same for ΔE_{3c} terms and the individual ΔE_{2c}(BC) terms which correspond to interactions between either the two water molecules or the water and benzene molecules. This shows respectively the rigid character of galanthamine (for a fixed conformation of the *N*-methyl group, axial or equatorial) and the relative independence of its interaction sites. This provides also some justifications for the good results yield by the MP2fit/DMA calculations which neglect molecular deformations and rely on pairwise potentials. In almost all cases, the model potential calculations give a fairly good estimate of the structures of the most significant complexes and the binding energies are predicted, for example in the case of the GALw + 2 H_2O system, in good agreement either with the LMP2 values or with the MPWB1K ones. Few complexes exhibit original structures arranged in molecular chains composed by the water molecule linked to the $N_{11}H^+$ group and the free water and benzene molecules. In these molecular arrangements, the relaxation energies due to the structuring are more sizable, as well as the ΔE_{3c} terms and the individual ΔE_{2c}(BC) terms which correspond to interactions between either the two water molecules or the water and benzene molecules. It is worth noting that the structures characterized by a molecular network above the $N_{11}H^+$ group show the largest binding energies, a feature justifying their interest for understanding the galanthamine behavior in molecular recognition processes.

Comparison with observations in the AChE binding site

The results of the cluster calculations in the isolated state have to be compared with the trends observed in the AChE binding site.

Figure 5 shows an overlay of the results obtained from the cluster calculations on the example of the GALw + 2 H_2O system and the galanthamine environment in the AChE binding site. It is seen that the main interaction sites of galanthamine predicted by the cluster calculations in the isolated state are indeed effective in the complex with AChE. Thus, the CH groups in the vicinity of the ammonium $N_{11}H^+$ which appear as one of the most representative and populated zone of interaction of the equatorial *N*-methyl conformer of galanthamine, are indeed involved in HB as HB donors with (1) the carboxylate group of Asp 72 (2) highly conserved water molecules (3) the π system of the indole ring of Trp 84. The other notable interacting fragment of galanthamine pointed out by the theoretical calculations for the relevant conformer is the hydroxyl group, which is engaged in HB interactions with (1) the carboxylate group of Glu 199 (2) highly conserved water molecules. Lastly, it is worth noticing that the position of the strictly conserved water molecule (no 820)

Table 3 Relative stabilities (δE kJ mol^{-1}) and binding energies (ΔE kJ mol^{-1}) of the most significant GALw + 2 H_2O complexes calculated at various levels of theory

Complex[a]	δE		ΔE			Proportion[b]
	LMP2	MPWB1K	LMP2	MPWB1K	MP2fit/DMA	
eq1:H_2O:H_2O	0.0	0.0	−61.1	−73.7	−65.1	9
ax1:H_2O:H_2O	3.4	3.6	−59.9	−72.0	−72.0	22
eq1:H_2O:$C_{10}H$–$C_{12}H$–$C_{17}H$	4.6	6.3	−56.5	−66.8	−61.3	26
ax1:H_2O:C_9H–$C_{10}H$	9.1	11.7	−54.2	−62.8	−59.2	20
ax3:H_2O:$O_{15}H$–O_4–O_{13}	12.8	17.2	−59.5	−69.6	–[c]	30
ax2:H_2O:$O_{15}H$	14.5	23.1	−58.6	−66.0	−68.1	36
ax1:H_2O:$C_{14}H$	17.3	22.4	−46.0	−52.7	−50.0	43
eq1:$C_{10}H$–$C_{12}H$–$C_{17}H$:C_2H	22.1	27.4	−39.0	−45.4	−37.9	47
eq3:$C_{10}H$–$C_{12}H$–$C_{17}H$:$O_{15}H$	22.5	29.8	−45.7	−52.0	–[c]	18
eq2:$C_{17}H$:$O_{15}H$	29.6	38.8	−39.1	−44.6	−47.1	11

[a] In the xn:i:j notations: x denotes the position (ax/eq) of the *N*-methyl substituent in the GAL subfragment; n denotes the conformation of the GAL subfragment with : intramolecular $O_{15}H_{16}$…O_4 HB (1), a *trans* orientation of the $O_{15}H$ group with respect to the C_5–C_6 bond (2), a *gauche* orientation of the $O_{15}H$ group with respect to the C_5–C_6 bond (3); i and j denote the GALw sites involved in the interaction with the two water molecules

[b] From the four intermolecular approaches (see "Method", model intermolecular potential calculations), highest proportion yielded by the MP2fit/DMA calculations for the considered complex

[c] The geometry optimized using the MPWB1K functional differs notably from the structure yielded by the MP2fit/DMA calculations, hence their binding energies could not be compared

Table 4 Relative stabilities (δE kJ mol^{-1}) and binding energies (ΔE kJ mol^{-1}) of the most significant GALw + H_2O + C_6H_6 complexes calculated at various levels of theory

Complex[a]	δE		ΔE			Proportion[b]
	LMP2	MPWB1K	LMP2	MPWB1K	MP2fit/DMA	
ax1:H_2O:H_2O	0.0	0.0	−65.5	−64.3	−66.5	18
eq1:H_2O:$C_{10}H$–$C_{12}H$–$C_{17}H$	2.2	2.1	−61.1	−60.4	−66.0	12
ax1:H_2O:C_9H–$C_{10}H$	6.6	6.6	−58.9	−57.6	−65.4	25
ax1:H_2O:arom. Ring	11.5	16.8	−54.0	−47.4	−67.2	26
ax1:H_2O:C_2H	14.0	10.5	−51.5	−53.7	−57.4	12
eq1:$C_{12}H$–$C_{17}H$:$C_{10}H$–$C_{12}H$–$C_{17}H$	16.0	16.3	−47.3	−45.8	−50.7	18
ax3:H_2O:$O_{15}H$	20.3	20.7	−54.2	−55.7	−62.6	30
ax2:H_2O:$O_{15}H$	22.2	23.5	−53.1	−54.5	−61.8	22
eq1:$C_{10}H$–$C_{12}H$–$C_{17}H$:C_2H	22.9	19.6	−40.4	−42.5	−42.8	21
eq3:$C_{12}H$–$C_{17}H$:$O_{15}H$	30.4	31.9	−40.0	−39.6	−44.8	20

[a] In the xn:i:j notations: x denotes the position (ax/eq) of the *N*-methyl substituent in the GAL subfragment; n denotes the conformation of the GAL subfragment with : intramolecular $O_{15}H_{16}$…O_4 HB (1), a *trans* orientation of the $O_{15}H$ group with respect to the C_5–C_6 bond (2), a *gauche* orientation of the $O_{15}H$ group with respect to the C_5–C_6 bond (3); i denotes the GALw site involved in the interaction with the water molecule; j denotes the GALw site involved in the interaction with the benzene molecule

[b] From the four intermolecular approaches (see "Method", model intermolecular potential calculations), highest proportion yielded by the MP2fit/DMA calculations for the considered complex

in the vicinity of the O_4, O_{13} and O_{14} atoms observed in galanthamine derivatives-AChE complexes[15, 22, 64] appears in close vicinity (Fig. 5) of two locations predicted by the calculations. In fact, most of the positions anticipated by the calculations that are not observed experimentally correspond to (1) binding of water molecules to interaction sites already occupied (e.g. with the water molecule bound to the $N_{11}H^+$ group of galanthamine) (2) secondary interaction sites (e.g. with the C_2H group of galanthamine as a HB donor) (Fig. 5). In order to quantify the agreement observed between the theoretical and observed positions of the water molecules, relevant complexes obtained among the most stable structures resulting from our theoretical calculations have been overlaid with the structure of galanthamine in the AChE binding site (1QTI PDB entry). The theoretical and experimental

structures of galanthamine have been overlaid on the heavy atoms (19 atomic pairs), the hydroxyle oxygen being not included owing to the significant proportion of theoretical GALw conformers with intramolecular $O_{15}H_{16}...O_4$ HB. The validity of our methodology is first assessed through the excellent agreement between the computed and experimental geometries of GALw, the rmsd of the superimpositions ranging between 0.096 and 0.351 Å. Furthermore, the interest of our approach is also illustrated through the values of the distances between the oxygen atoms of the predicted and observed water molecules. Thus, these distances are of 1.4 and 1.9 Å with respect to the oxygen atoms of crystal water molecules nos 764 and 706 (see Figs. 5, 6). A greater value of 2.9 Å is obtained for the same parameter considering another theoretical position with respect to the oxygen atom of crystal water molecule no 803. This difference is due to the fact that the predicted water molecule is located symetrically between the $C_{10}H$ and $C_{17}H$ groups, whereas the observed one is closer to the $C_{17}H$ group in the AChE binding site environment. The best agreement is observed for the crystal water molecule no 820, the distance between the oxygen atoms of the predicted and observed positions being of 1.0 Å. Finally, it is worth noting that one water molecule predicted by the cluster calculations is located at 0.6 Å of a carboxylate oxygen atom of Glu 199.

A more detailed view of the superimposition of the theoretical and experimental results is shown in Fig. 6. This view, focussed on the ammonium moiety of GALw represented by the $N_{11}H^+$ group and the $C_{10}H$, $C_{12}H$ and $C_{17}H$ groups, shows that this part of GALw concentrates an important proportion of the interactions. Thus, almost all water molecules in the immediate surroundings of the cationic head of GALw interact as HBA. However, it is worth noting from Fig. 6 that the number of positions predicted by the calculations is more important that the positions really occupied in the AChE active site, an observation that reflects the effect of the AChE active site local environment.

Figure 7 shows the overlay of the theoretical results obtained from the cluster calculations for the GALw + H_2O + C_6H_6 system and the galanthamine environment in the AChE binding site. Indeed, it is worth reminding that during the theoretical exploration of the PES of interaction of GALw with the water and benzene molecules, the two fragments are in competition for interacting with GALw. As a result, some of the positions predicted by the theoretical calculations are occupied both by water and benzene molecules. For more clarity of Fig. 7, water molecules occupying the same positions than benzene molecules have therefore been removed. In this paragraph, we will focus on the comparison of the benzene molecules positions since those corresponding to water

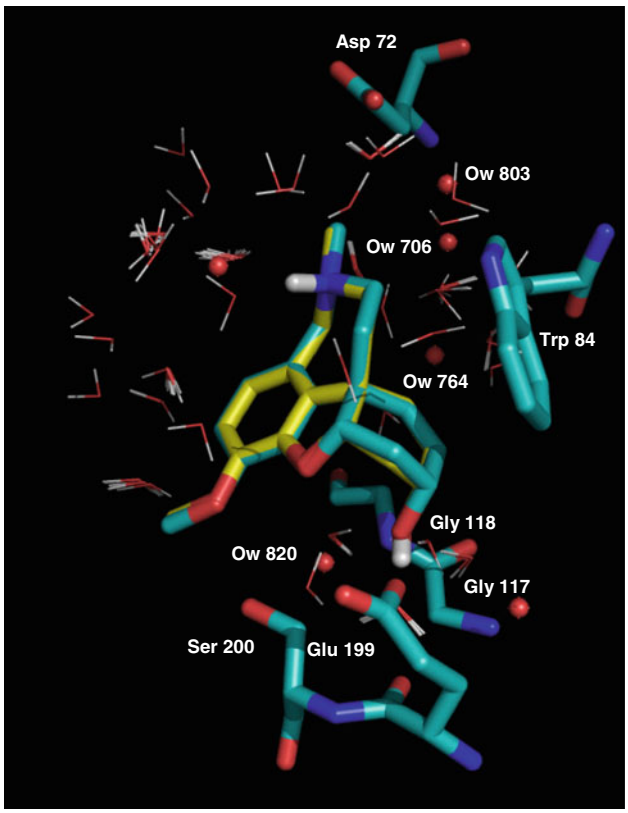

Fig. 5 Superimposition of the theoretical results obtained through the cluster calculations (Galw + $2H_2O$) to the galanthamine environment in the AChE binding site (1QTI entry, the galanthamine fragments have been overlaid). The numbering of relevant amino acids, represented in sticks, and of crystal water molecules, represented as *red spheres*, is indicated

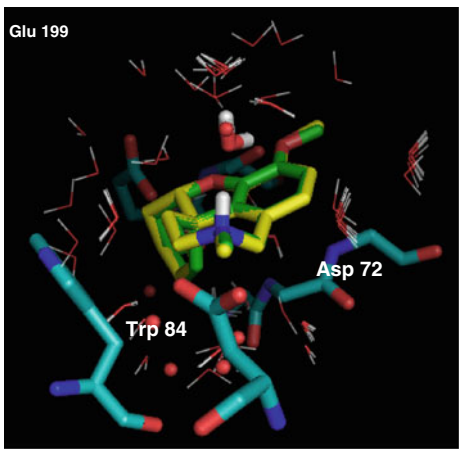

Fig. 6 Detailed view, in the direction of the cationic head of GALw, of the superimposition of the theoretical results obtained through the cluster calculations (GALw + 2 H_2O) to the galanthamine environment in the AChE binding site (1QTI entry, the galanthamine fragments have been overlaid). The numbering of relevant amino acids, represented in sticks, and of crystal water molecules, represented as *red spheres*, is indicated

molecules have been compared in the previous sub-section. First, a significant proportion of the sites predicted by the theoretical calculations for benzene molecules are indeed occupied by lateral chain of aromatic residues in the AChE binding site (Fig. 7). This is particularly remarkable for Trp84, this residue being reported as the main one ensuring the stabilization of the substrate in the active site [17]. This is also true for (1) Tyr121 and Phe330 which belong to the CAS and form the bottleneck of the gorge that leads to the active site[17] (2) for Phe290 which contributes to the acyl pocket which determines the specificity for acetylcholine [21]. In fact, the aromatic ring of Phe330 is found in close contact with the Galw water molecule (distance of 3.5 Å between the water oxygen atom and the centroid of the Phe330 ring). This position of the Phe330 aromatic ring is from our point of view also especially noticeable since it is in line with the major role in molecular interactions predicted by the theoretical calculations for the water molecule linked to the GALw $N_{11}H^+$ group, acting as a HBD, a trend that appear confirmed in the AChE binding site. Lastly, Tyr334, one of the fourteen aromatic residues highly conserved according to the species, is localized nearby (from about 2 to 3 Å) the various theoretical positions. According to the aromatic residues considered, it is worth noticing that the ring orientation between the theoretical and experimental positions can be significantly different. For Tyr84 and Phe330 the ring orientation is very similar whereas for Tyr121, Phe290 and Phe331, a significant change of orientation is noticeable on Fig. 7. These trends are in line with the flexibility of the aromatic residues of AChE as it has been pointed out from X-ray crystallography and molecular dynamics simulations [21]. One can also notice that theoretical positions corresponding to stacking interactions with the aromatic ring of the anisole fragment are not occupied in the AChE binding site. As already discussed in the previous paragraph for water molecules, this might reflect the influence of the local environment of the AChE binding site, occupied by other residues fulfilling this role.

To quantify the agreement between the predicted and observed positions of the aromatic rings, as in the previous sub-section for water molecules, relevant complexes obtained among the most stable structures resulting from our theoretical calculations have been overlaid with the structure of galanthamine in the AChE binding site (1QTI PDB entry). First, it is worth noticing that the centroid of the benzene ring of a predicted position appears located at 0.65 Å of a crystal water molecule (no 706). Furthermore, the agreement between the theoretical and experimental positions is also assessed through the distances between the centroids of the corresponding aromatic rings. Thus, this parameter has a value of 1.1 Å with respect to the centroid of Phe290, the angle between the aromating ring planes of the computed and observed positions being of 44°. Similarly, the same distance has a value of 2.8 Å with respect to the centroid of Phe330 for another predicted theoretical position, the angle between the aromatic ring planes of the computed and observed positions being of 6°.

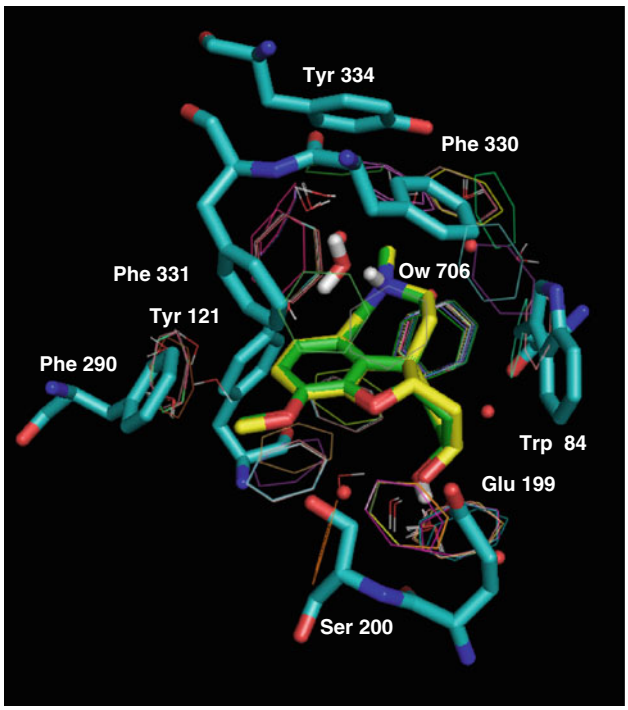

Fig. 7 Superimposition of the theoretical results obtained through the cluster calculations (Galw + H_2O + C_6H_6) to the galanthamine environment in the AChE binding site (1QTI entry, the galanthamine fragments have been overlaid). The numbering of relevant amino acids, in particular aromatic residues, represented in sticks, and of cristallographic water molecules, shown as *red spheres*, is indicated

Conclusion

A thorough mapping of the interaction sites of the anti-Alzheimer drug galanthamine has been realized from a theoretical approach based on the use of an intermolecular pairwise potential allowing an exhaustive exploration of the PES of interaction with benzene and water molecules and quantum chemistry calculations on the most relevant complexes. Our results show clearly the influence of the initial distance separating the fragments in the nature of the complexes formed. Contrarily to what one might expect from chemical intuition, galanthamine behaves mainly as a HB donor. The conformation of galanthamine has also a strong impact in the type of complexes formed. In particular, the axial or equatorial orientation of the *N*-methyl substituent leads to significantly different complexes. The axial orientation of the methyl substituent leads essentially

to one type of complexes, established from HB interactions with the water molecule neutralizing the positive charge of the ammonium $N_{11}H^+$. Remarkably, the equatorial orientation of this substituent induces significantly different complexes, the molecule being much more potent in terms of interaction and binding to AChE. Among the various HB donor groups of the molecule, CH groups, that can be divided in two categories, are found to play a key role. The first category corresponds to alkyl groups located in the vicinity of the positively charged ammonium and the second one is formed with the aromatic anisole and ethylenic CH. When compared to the results obtained with the subsequent DFT and ab initio calculations, the MP2fit/DMA intermolecular potential models are found to give good results, both from an energetic and geometric point of view. This is mainly due to the rigid structure of galanthamine and the relative independence of its interaction sites. The comparison of the results obtained from the cluster calculation in the isolated state to the experimental observations in the binding site of AChE shows a good agreement. The positions of crystallographic water molecules are notably predicted by the cluster calculations. This methodology appears therefore promising for the discrimination of water interaction sites of biological ligands. Furthermore, the position of aromatic groups of aminoacids recognized as prominent in the function of AChE is in concordance with the positions predicted by the cluster calculations. It is worth noticing that the positions for which a significantly different orientation of the aromatic ring are observed coincide with AChE active site gorge aminoacids identified as flexible. The strategy presented in this work can therefore be applied to the quantitative deciphering of the molecular interactions of important biological ligands. In the case of AChE inhibitors based on galanthamine derivatives, it provides relevant information for rational drug-design.

Acknowledgments This work was granted access to the HPC resources of [CCRT/CINES/IDRIS] under the allocation c2011085117 made by GENCI (Grand Equipement National de Calcul Intensif). The authors gratefully acknowledge the CCIPL (Centre de Calcul Intensif des Pays de la Loire) for grants of computer time. S. K. thank the AUF (Agence Universitaire de la Francophonie) for financial support and the LCOS (Laboratoire de Chimie Organique Structurale) of Abidjan Cocody University for its help.

References

1. Bartus RT, Dean RL III, Beer B, Lippa AS (1982) The cholinergic hypothesis of geriatric memory dysfunction. Science 217(4558):408–414
2. Dunnett SB, Fibiger HC (1993) Role of forebrain cholinergic systems in learning and memory: relevance to the cognitive deficits of aging and Alzheimer's dementia. Prog Brain Res 98:413–420
3. Bartus RT (2000) On neurodegenerative diseases, models, and treatment strategies: lessons learned and lessons forgotten a generation following the cholinergic hypothesis. Exp Neurol 163(2):495–529
4. Arneric SP, Holladay MW (2000) Agonists and antagonists of nicotinic acetylcholine receptors. Handbook of experimental pharmacology. Neuronal Nicotinic Receptors 144:419–453
5. Bertrand D, Gopalakrishnan M (2007) Allosteric modulation of nicotinic acetylcholine receptors. Biochem Pharmacol 74:1155–1163
6. Weinstock M, Razin M, Chorev M, Enz A (1994) Pharmacological evaluation of phenyl-carbamates as CNS-selective acetylcholinesterase inhibitors. J Neural Transmission (Neuroprotection in Neurodegeneration) Supplement 43:219–225
7. Bar-On P, Millard CB, Harel M, Dvir H, Enz A, Sussman JL, Silman I (2002) Kinetic and structural studies on the interaction of cholinesterases with the anti-alzheimer drug rivastigmine. Biochemistry 41(11):3555–3564
8. Wang YE, Yue DX, Tang XC (1986) Anti-cholinesterase activity of huperzine A. Acta Pharmacol Sin 7(2):110–113
9. Kozikowski AP, Thiels E, Tang XC, Hanin I (1992) Huperzine A. A possible lead structure in the treatment of Alzheimer's disease. Adv Med Chem 1:175–205
10. Kawakami Y, Inoue A, Kawai T, Wakita M, Sugimoto H, Hopfinger AJ (1996) The rationale for E2020 as a potent acetylcholinesterase inhibitor. Bioorg Med Chem 4(9):1429–1446
11. Kryger G, Silman I, Sussman JL (1999) Structure of acetylcholinesterase complexed with E2020 (Aricept): implications for the design of new anti-Alzheimer drugs. Structure (London) 7(3):297–307
12. Rogawski MA, Wenk GL (2003) The neuropharmacological basis for the use of memantine in the treatment of Alzheimer's disease. CNS Drug Rev 9(3):275–308
13. Jia P, Sheng R, Zhang J, Fang L, He Q, Yang B, Hu Y (2009) Design, synthesis and evaluation of galanthamine derivatives as acetylcholinesterase inhibitors. Eur J Med Chem 44(2):772–784
14. Vanlaer S, De Borggraeve WM, Voet A, Gielens C, De Maeyer M, Compernolle F (2008) Spirocyclic pyridoazepine analogues of galanthamine: synthesis, modelling studies and evaluation as inhibitors of acetylcholinesterase. Eur J Org Chem 15:2571–2581
15. Bartolucci C, Haller LA, Jordis U, Fels G, Lamba D (2010) Probing Torpedo californica acetylcholinesterase catalytic gorge with two novel bis-functional galanthamine derivatives. J Med Chem 53(2):745–751
16. Dvir H, Silman I, Harel M, Rosenberry TL, Sussman JL (2010) Acetylcholinesterase: from 3D structure to function. Chem-Biol Interact 187(1–3):10–22
17. Silman I, Sussman JL (2008) Acetylcholinesterase: how is structure related to function? Chem-Biol Interact 175(1–3):3–10
18. Nascimento ECM, Martins JBL, dos Santos ML, Gargano R (2008) Theoretical study of classical acetylcholinesterase inhibitors. Chem Phys Lett 458(4–6):285–289
19. de Paula AAN, Martins JBL, dos Santos ML, Nascente LdC, Romeiro LAS, Areas TFMA, Vieira KST, Gamboa NF, Castro NG, Gargano R (2009) New potential AChE inhibitor candidates. Eur J Med Chem 44(9):3754–3759
20. Nascimento ECM, Martins JBL (2011) Electronic structure and PCA analysis of covalent and non-covalent acetylcholinesterase inhibitors. J Mol Model 17(6):1371–1379
21. Xu Y, Colletier J-P, Weik M, Jiang H, Moult J, Silman I, Sussman JL (2008) Flexibility of aromatic residues in the active-site gorge of acetylcholinesterase: X-ray versus molecular dynamics. Biophys J 95(5):2500–2511

22. Greenblatt HM, Kryger G, Lewis T, Silman I, Sussman JL (1999) Structure of acetylcholinesterase complexed with (-)-galanthamine at 2.3.ANG. resolution. FEBS Lett 463(3):321–326
23. Greenblatt HM, Guillou C, Guenard D, Argaman A, Botti S, Badet B, Thal C, Silman I, Sussman JL (2004) The complex of a bivalent derivative of galanthamine with torpedo acetylcholinesterase displays drastic deformation of the active-site Gorge: implications for structure-based drug design. J Am Chem Soc 126(47):15405–15411
24. Koellner G, Kryger G, Millard CB, Silman I, Sussman JL, Steiner T (2000) Active-site gorge and buried water molecules in crystal structures of acetylcholinesterase from Torpedo californica. J Mol Biol 296(2):713–735
25. Xu Y, Shen J, Luo X, Silman I, Sussman JL, Chen K, Jiang H (2003) How does Huperzine A enter and leave the binding Gorge of acetylcholinesterase? Steered molecular dynamics simulations. J Am Chem Soc 125(37):11340–11349
26. Babakhani A, Talley TT, Taylor P, McCammon JA (2009) A virtual screening study of the acetylcholine binding protein using a relaxed-complex approach. Comput Biol Chem 33(2):160–170
27. Cheng YH, Cheng XL, Radic Z, McCammon JA (2008) Acetylcholinesterase: mechanisms of covalent inhibition of H447I mutant determined by computational analyses. Chem-Biol Interact 175(1–3):196–199
28. Cheng YH, Cheng XL, Radic Z, McCammon JA (2007) Acetylcholinesterase: mechanisms of covalent inhibition of wild-type and H447I mutant determined by computational analyses. J Am Chem Soc 129(20):6562–6570
29. Senapati S, Cheng YH, McCammon JA (2006) In situ synthesis of a tacrine-triazole-based inhibitor of acetylcholinesterase: configurational selection imposed by steric interactions. J Med Chem 49(21):6222–6230
30. Bui JM, Tai K, McCammon JA (2004) Acetylcholinesterase: enhanced fluctuations and alternative routes to the active site in the complex with Fasciculin-2. J Am Chem Soc 126(23): 7198–7205
31. Kua J, Zhang Y, Eslami AC, Butler JR, McCammon JA (2003) Studying the roles of W86, E202, and Y337 in binding of acetylcholine to acetylcholinesterase using a combined molecular dynamics and multiple docking approach. Protein Sci 12(12): 2675–2684
32. Henchman RH, McCammon JA (2002) Structural and dynamic properties of water around acetylcholinesterase. Protein Sci 11(9):2080–2090
33. Kone S, Galland N, Bamba E-HS, Le Questel J-Y (2008) Hydrogen-bonding properties of galanthamine: an investigation through crystallographic database observations and computational chemistry. Acta Cryst B B64(3):338–347
34. Kone S, Galland N, Graton J, Illien B, Laurence C, Guillou C, Le Questel J-Y (2006) Structural features of neutral and protonated galanthamine: a crystallographic database and computational investigation. Chem Phys 328(1–3):307–317
35. Atkinson AP, Baguet E, Galland N, Le Questel JY, Planchat AP, Graton J (2011) Structural features and hydrogen-bond properties of galanthamine and codeine: an experimental and theoretical study. Chem Eur J 17:11637–11649
36. van Mourik T, Price SL, Clary DC (2001) Diffusion Monte Carlo simulations on uracil-water using an anisotropic atom-atom potential model. Faraday Discus (Cluster Dynamics) 118:95–108
37. Stone AJ (1981) Distributed multipole analysis, or how to describe a molecular charge distribution. Chem Phys Lett 83(2): 233–239
38. Stone AJ, Alderton M (1985) Distributed multipole analysis methods and applications. Mol Phys 56(5):1047–1064
39. Rueter LE, Anderson DJ, Briggs CA, Donnelly-Roberts DL, Gintant GA, Gopalakrishnan M, Lin N-H, Osinski MA, Reinhart GA, Buckley MJ, Martin RL, McDermott JS, Preusser LC, Seifert TR, Su Z, Cox BF, Decker MW, Sullivan JP (2004) ABT-089: pharmacological properties of a neuronal nicotinic acetylcholine receptor agonist for the potential treatment of cognitive disorders. CNS Drug Rev 10(2):167–182
40. Williams DE, Cox SR (1984) Nonbonded potentials for azahydrocarbons: the importance of the Coulombic interaction. Acta Crystallograph Sect B 40(4):404–417
41. Mitchell JBO, Price SL (1990) The nature of the N-H O:C hydrogen bond: an intermolecular perturbation theory study of the formamide/formaldehyde complex. J Comput Chem 11(10): 1217–1233
42. Stone JA (2003) GDMA: a program for performing distributed multipole analysis of wavefunctions calculated by the Gaussian system of programs, version 1.3, University of Cambridge (UK)
43. Stone AJDAE, Fraschini E, Hodges MP, Meredith AW, Popelier PLA, Wales DJ (2001) ORIENT, 4.4 edn. University of Cambridge. Cambridge
44. Braun DE, Tocher DA, Price SL, Griesser UJ (2012) The complexity of hydration of phloroglucinol: a comprehensive structural and thermodynamic characterization. J Phys Chem B 116(13):3961–3972. doi:10.1021/jp211948q
45. Tsuzuki S, Uchimaru T, Mikami M (2012) Magnitude of CH/O interactions between carbohydrate and water. Theoretical Chemistry Accounts 131 (3). doi:10.1007/s00214-012-1192-0
46. Hamaguchi N, Fusti-Molnar L, Wlodek S (2012) Force-field and quantum-mechanical binding study of selected SAMPL3 host-guest complexes. J Comput Aided Mol Des 26(5):577–582
47. Zhao Y, Truhlar DG (2004) Hybrid meta density functional theory methods for thermochemistry, thermochemical kinetics, and noncovalent interactions: the MPW1B95 and MPWB1K models and comparative assessments for hydrogen bonding and van der Waals interactions. J Phys Chem A 108(33):6908–6918
48. Zhao Y, Truhlar DG (2005) Benchmark databases for nonbonded interactions and their use to test density functional theory. J Chem Theory Comput 1(3):415–432
49. Zhao Y, Truhlar DG (2007) Density functionals for noncovalent interaction energies of biological importance. J Chem Theory Comput 3(1):289–300
50. Gil A, Branchadell V, Bertran J, Oliva A (2007) CH/pi interactions in DNA and proteins. A theoretical study. J Phys Chem B 111(31):9372–9379
51. Dkhissi A, Blossey R (2007) Performance of DFT/MPWB1K for stacking and H-bonding interactions. Chem Phys Lett 439(1–3):35–39
52. Frisch MJ, Trucks GW, Schlegel HB, Scuseria GE, Robb MA, Cheeseman JR, Montgomery JA, Vreven JT, N. KK, Burant JC, Millam JM, Iyengar SS, Tomasi J, Barone V, Mennucci B, Cossi M, Scalmani G, Rega N, Petersson GA, Nakatsuji H, Hada M, Ehara M, Toyota K, Fukuda R, Hasegawa J, Ishida M, Nakajima T, Honda Y, Kitao O, Nakai H, Klene M, Li X, Knox JE, Hratchian HP, Cross JB, Adamo C, Jaramillo J, Gomperts R, Stratmann RE, Yazyev O, Austin AJ, Cammi R, Pomelli C, Ochterski JW, Ayala PY, Morokuma K, Voth GA, Salvador P, Dannenberg JJ, Zakrzewski VG, Dapprich S, Daniels AD, Strain MC, Farkas O, Malick DK, Rabuck AD, Raghavachari K, Foresman JB, Ortiz JV, Cui Q, Baboul AG, Clifford S, Cioslowski J, Stefanov BB, Liu G, Liashenko A, Piskorz P, Komaromi I, Martin RL, Fox DJ, Keith T, Al-Laham MA, Peng CY, Nanayakkara A, Challacombe M, Gill PMW, Johnson B, Chen W, Wong MW, Gonzalez C, Pople JA (2004) Gaussian 03, Revision C.02. Gaussian 03, Revision C02, Gaussian Inc, Wallingford CT, 2004
53. Boys SF, Bernardi F (1970) The calculation of small molecular interactions by the differences of separate total energies. Some procedures with reduced errors. Mol Phys 19(4):553–566
54. Xantheas SS (1996) On the importance of the fragment relaxation energy terms in the estimation of the basis set superposition error

correction to the intermolecular interaction energy. J Chem Phys 104(21):8821–8824
55. Pulay P, Saeboe S (1986) Orbital-invariant formulation and second-order gradient evaluation in Moeller-Plesset perturbation theory. Theor Chim Acta 69(5–6):357–368
56. Saebo S, Pulay P (1993) Local treatment of electron correlation. Annu Rev Phys Chem 44:213–236
57. Saebo S, Tong W, Pulay P (1993) Efficient elimination of basis-set-superposition errors by the local correlation method: accurate ab initio studies of the water dimer. J Chem Phys 98(3):2170–2175
58. Hampel C, Werner H-J (1996) Local treatment of electron correlation in coupled cluster theory. J Chem Phys 104(16):6286–6297
59. Pedulla JM, Vila F, Jordan KD (1996) Binding energy of the ring form of (H2O)6: comparison of the predictions of conventional and localized-orbital MP2 calculations. J Chem Phys 105(24): 11091–11099
60. Hill JG, Platts JA, Werner H-J (2006) Calculation of intermolecular interactions in the benzene dimer using coupled-cluster and local electron correlation methods. Phys Chem Chem Phys 8(35):4072–4078
61. Jaguar, version 7.0 (2007) Schrödinger, LLC, New York
62. Xantheas SS (1994) Ab initio studies of cyclic water clusters (H2O)n, n = 1-6. II. Analysis of many-body interactions. J Chem Phys 100(10):7523–7534
63. Delano WL (2004) The Pymol molecular graphics system, http://www.pymol.org. Delano Scientific, San Carlos
64. Bartolucci C, Perola E, Pilger C, Fels G, Lamba D (2001) Three-dimensional structure of a complex of galanthamine (nivalin) with acetylcholinesterase from Torpedo californica: implications for the design of new anti-Alzheimer drugs. Proteins Struct Funct Genet 42(2):182–191
65. Stanca-Kaposta EC, Gamblin DP, Cocinero EJ, Frey J, Kroemer RT, Fairbanks AJ, Davis BG, Simons JP (2008) Solvent interactions and conformational choice in a core N-glycan segment: gas phase conformation of the central, branching Trimannose unit and its singly hydrated complex. J Am Chem Soc 130(32): 10691–10696
66. van Mourik T (2008) Assessment of density functionals for intramolecular dispersion-rich interactions. J Chem Theory Comput 4(10):1610–1619
67. Jensen F (2010) An atomic counterpoise method for estimating inter- and intramolecular basis set superposition errors. J Chem Theory Comput 6(1):100–106
68. Schuetz M, Rauhut G, Werner H-J (1998) Local treatment of electron correlation in molecular clusters: structures and stabilities of (H2O)n, n = 2–4. J Phys Chem A 102(29):5997–6003
69. Sponer J, Riley KE, Hobza P (2008) Nature and magnitude of aromatic stacking of nucleic acid bases. Phys Chem Chem Phys 10(19):2595–2610
70. Zhao Y, Truhlar DG (2008) Density functionals with broad applicability in chemistry. Acc Chem Res 41(2):157–167